

1 Visible-Light-Driven Triplet Sensitization of Polycyclic Aromatic 2 Hydrocarbons Using Thionated Perinones

3 Jonathan R. Palmer, Kaylee A. Wells, James E. Yarnell, Joseph M. Favale, and Felix N. Castellano*



Cite This: <https://dx.doi.org/10.1021/acs.jpcllett.0c01634>



Read Online

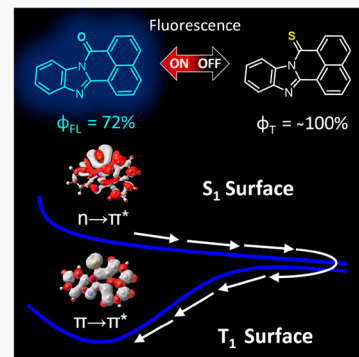
ACCESS |

Metrics & More

Article Recommendations

Supporting Information

4 **ABSTRACT:** Metal-free chromophores that efficiently generate triplet excited states
5 represent promising alternatives with respect to transition metal-containing photosensitizers,
6 such as those featuring metal-to-ligand charge transfer excited states. However, such molecular
7 constructs have remained underexplored due to the unclear relationship(s) between molecular
8 structure and efficient/rapid intersystem crossing. In this regard, we present a series of three
9 thionated perinone chromophores serving as a newly conceived class of heavy metal-free triplet
10 photosensitizers. We demonstrate that thionation of the lone C=O substituent in each highly
11 fluorescent perinone imparts red-shifted absorbance bands that maintain intense extinction
12 coefficients across the visible spectrum, as well as unusually efficient triplet excited state
13 formation as inferred from the measured singlet O₂ quantum yields at 1270 nm ($\Phi_{\Delta} = 0.78 - 1.0$).
14 Electronic structure calculations revealed the emergence of a low energy S₁ ($n \rightarrow \pi^*$) excited state
15 in the proximity of a slightly higher energy S₂ ($\pi \rightarrow \pi^*$) excited state. The distinct
16 character in each of the two lowest-lying singlet state manifolds resulted in the energetic
17 inversion of the corresponding triplet excited states due to differences in electron exchange
18 interactions. Rapid S₁ → T₁ intersystem crossing was thereby facilitated in this manner through spin-orbit coupling as predicted by
19 the El Sayed rules. The lifetimes of the resultant triplet excited states persisted into the microsecond time regime, as measured by
20 transient absorbance spectroscopy, enabling effective bimolecular triplet sensitization of some common polycyclic aromatic
21 hydrocarbons. The synthetically facile interchange of a single O atom to an S atom in the investigated perinones resulted in marked
22 changes to their photophysical properties, namely, conversion of dominant singlet state fluorescence in the former to long-lived
23 triplet excited states in the latter. The combined results suggest a general strategy for accessing long-lived triplet excited states in
24 organic chromophores featuring a lone C=O moiety residing within its structure, valuable for the design of metal-free triplet
25 photosensitizers.



26 **P**olycyclic aromatic hydrocarbons (PAHs) have been
27 intensively studied over the past several decades and are
28 well-known for their valuable optical and electronic proper-
29 ties.¹ Among their applications, PAHs have recently exhibited
30 increasing potential in photocatalysis and solar energy
31 conversion schemes.^{2–9} The triplet excited states of PAHs
32 have become the focal point of these photoinitiated processes,
33 where they are largely used in bimolecular chemical trans-
34 formations associated with triplet-triplet annihilation upcon-
35 version^{2–6} (TTA-UC) or photoredox catalysis.^{7–9} In many
36 PAHs, triplet states are inherently difficult to generate through
37 direct excitation due to the large singlet-triplet splitting in
38 these chromophores.¹ A limited number of PAHs are capable
39 of singlet fission, where two triplet excited states are produced
40 from the fission of one high-energy singlet state.¹⁰ However,
41 observation of this phenomenon in PAHs has been restricted
42 to tetracene,¹¹ pentacene,¹² and some of their derivatives,^{13,14}
43 which feature the proper singlet/triplet energetics (2T₁ < S₁).
44 Thus, most PAHs often require triplet sensitization through
45 direct Dexter-type triplet energy transfer (TET) to efficiently
46 access their triplet manifold.⁴

Currently, most triplet sensitizers incorporate second- and 47
third-row transition metals to promote triplet formation 48
because the spin-orbit coupling (SOC) constant is approx- 49
imately proportional to the square of atomic number Z.^{15–19} 50
However, the simplest and most easily accessible of these 51
molecules absorb intensely in the ultraviolet region and suffer 52
from smaller visible absorption cross sections,^{3,15,18,20,21} 53
limiting their potential in solar-light-driven applications.⁵⁴
Additionally, the strong SOC that results from the heavy- 55
atom effect also drastically shortens triplet lifetimes compared 56
to those of many organic chromophores.^{15,18} 57
Many investi- 58
gations have attempted to circumvent these issues by 59
appending organic chromophores within the ligand framework,⁵⁹
which strategically introduces a series of energy transfer 60

Received: May 26, 2020

Accepted: June 9, 2020

Published: June 9, 2020

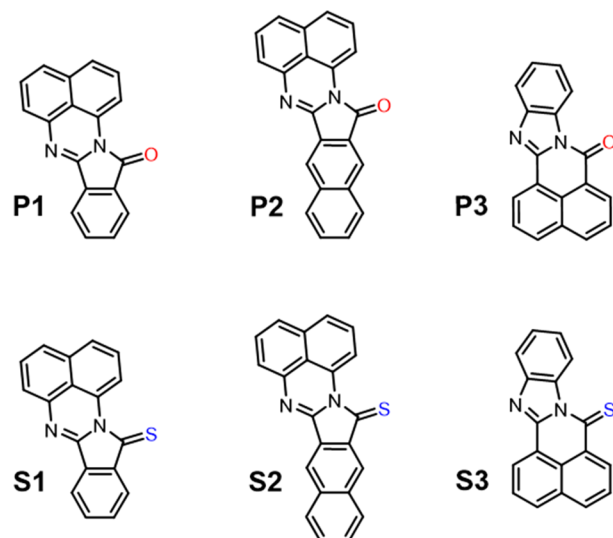
61 cascades and triplet state thermal equilibria to achieve
 62 enhanced visible-light harvesting and extended triplet life-
 63 times.^{15,18,22–26} However, these bi- and polychromophoric
 64 transition metal architectures can be very cumbersome and
 65 tedious to design and synthesize, where it is also difficult to
 66 predict and control the achieved thermal equilibrium process
 67 and the resultant lifetime extension *a priori*.²³ Among the
 68 previously mentioned obstacles, the significant cost and
 69 relatively low natural abundance of the second- and third-
 70 row transition metals typically used in these constructs limit
 71 the practicality of these systems for large-scale applications.
 72 Thus, there is substantial interest in generating easily accessible
 73 organic triplet photosensitizers featuring strong visible
 74 absorbing cross sections, long excited state lifetimes, and
 75 redox properties amenable for photoredox catalysis.

76 Recently, Scholes and co-workers demonstrated that
 77 thionation of perylenediimides (PDIs) resulted in subpico-
 78 second intersystem crossing (ISC) time constants, represent-
 79 ing one of the few reported totally organic PDI derivatives with
 80 efficient access to its triplet manifold.²⁷ Because the rate of ISC
 81 was independent of the degree of PDI thionation, they
 82 concluded that the heavy-atom effect was not the cause of the
 83 increased SOC, but rather the energetic proximity of many of
 84 the low-lying singlet and triplet excited states. This principle
 85 has since been extended to a few thionated naphthalimide
 86 (NI) derivatives, which served as effective heavy-atom-free
 87 photosensitizers in photodynamic therapy (PDT).^{28–30} Sim-
 88 ilarly, Stryland and co-workers have pioneered a new class of
 89 thionated squarine dyes that also show promise as organic
 90 photosensitizers,^{31,32} resulting in their implementation in red-
 91 to-yellow upconversion schemes using rubrene as an acceptor/
 92 annihilator.³³ Thus, regardless of the core molecular frame-
 93 work, thionating various aromatic pendant carbonyl groups
 94 opens channels for efficient intersystem crossing to the triplet
 95 state without relying on the heavy-atom effect imparted by
 96 transition metals. While this is the case, aromatic thiones
 97 remain relatively underexplored as triplet sensitizers, with the
 98 currently available classes of molecules being restricted to the
 99 few examples discussed above.^{28,32,33}

100 Perinones and other polycyclic benzimidazole chromo-
 101 phores have emerged within the past decade as promising
 102 analogues of the ubiquitous PDI chromophores, finding
 103 increasing use in the dye industry^{34,35} and as organic n-type
 104 semiconductor materials.^{34,36–38} This newly found interest
 105 results from their synthetic simplicity, improved visible
 106 absorption capabilities,^{34,36–38} significant electron mobili-
 107 ties,^{36,37,39} and exceptional photochemical and thermal
 108 stabilities.^{34,35,40} Additionally, perinones can be easily accessed
 109 through solid state condensation and direct sublimation,³⁸
 110 generating chromophores with intense visible-light absorption
 111 prepared under solvent-free “green” synthetic conditions
 112 featuring limited material and purification costs. While these
 113 properties are ideal for realizing inexpensive organic triplet
 114 photosensitizers, perinones, much like PAHs, have limited
 115 access to their triplet manifolds. Akin to the photophysics in
 116 PDIs, the excited state evolution of perinones exclusively
 117 proceeds through short-lived singlet excited states with
 118 enormous fluorescence quantum yields.^{36,38}

119 In this investigation, we hypothesized that the photophysical
 120 tunability of perinone chromophores would echo those of
 121 PDIs and postulated that metal-free triplet photosensitizers
 122 could be generated on the basis of thionation at their lone
 123 carbonyl moiety [S1–S3 (Chart 1)]. It is worth noting that in

Chart 1. Molecular Structures of the Parent Perinones (P1–P3) and Thioperinones (S1–S3) Investigated in This Study



comparison to the thionated PDI and NI derivatives, the presence of a single carbonyl group in perinones completely eliminates regioselectivity issues in the thionation process, whereas both PDIs and NIs produce mixtures of multi-thionated products.^{27,41} Furthermore, the selected parent perinones [P1–P3 (Chart 1)] are capable of intense light absorption across the majority of the visible spectrum (400–600 nm), which significantly red-shifted in the visible region upon thionation. Thus, flexibility was enabled in terms of the visible excitation wavelength when these sensitizers were paired with common PAH acceptors. We demonstrate that PAH acceptors with triplet energies of up to ~1.8 eV could effectively be sensitized with diffusion-limited TET rates, which included tetracene, perylene, and 9,10-diphenylanthracene. Furthermore, we examined the nature of the electronic structure that facilitates efficient triplet formation in thionated perinones using electronic structure calculations.

The molecular structures of all the chromophores investigated in this study are presented in Chart 1, while all synthetic and characterization data are reported in the Supporting Information. We note that P1 and P3 have been previously synthesized and characterized,^{36,38} while P2 is a newly reported molecule. The normalized electronic absorption spectra measured in toluene of S1–S3 and their corresponding perinone precursors (P1–P3) are presented in Figure 1, with other relevant measured photophysical data summarized in Table 1. The lowest energy absorption bands of P1–P3 have previously been assigned as $^1(\pi \rightarrow \pi^*)$.³⁸ As presented in Figure 1, the lowest energy absorption bands of S1–S3 have similarly structured absorption envelopes with respect to their parent chromophores but display significant bathochromic shifts. The similarity within each absorption envelope suggests that the experimentally observed lowest energy electronic transition for each thionated perinone is also $^1(\pi \rightarrow \pi^*)$ in nature, with vibronic coupling that is not significantly perturbed upon thionation. The significant redshift observed upon thionation (>50 nm) is well-documented in the literature^{27,42,43} and can be rationalized by the significant energetic lowering of the lowest unoccupied molecular orbital (LUMO), while the highest occupied molecular orbital (HOMO) remains unchanged in energy (Table S1).

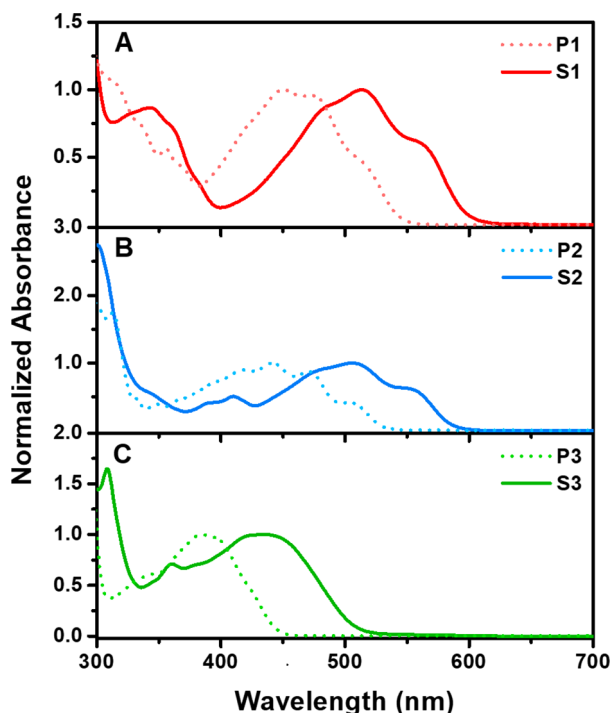


Figure 1. Normalized absorbance spectra (solid) of (A) S1, (B) S2, and (C) S3 overlaid with the corresponding normalized absorbance spectra (dashed) of P1–P3 in toluene.

Table 1. Absorbance and Photophysical Data of the Chromophores Used in This Study^a

molecule	$\lambda_{\text{abs max}}$ (nm) [ϵ ($M^{-1} \text{ cm}^{-1}$)] ^b	Φ_{PL} (298 K)	τ_{PL} (298 K) (ns)
P1	449 (8200)	0.046 ^c	1.00 ^f
S1	514 (10800)	<0.001 ^{c,e}	—
P2	442 (11300)	0.091 ^c	1.51 ^f
S2	507 (8700)	<0.001 ^{c,e}	—
P3	385 (11700)	0.72 ^d	10.7 ^f
S3	435 (9900)	<0.001 ^{d,e}	—

^aMeasurements were performed in toluene. ^bMolar extinction coefficients determined for the lowest energy $\lambda_{\text{abs max}}$. ^cQuantum yields measured using aerated $[\text{Ru}(\text{bpy})_3](\text{PF}_6)_2$ in acetonitrile as the standard ($\lambda_{\text{em}} = 621 \text{ nm}$; $\Phi_{\text{PL}} = 0.018$).⁴⁴ ^dQuantum yield measured using 4-aminonaphthalene-1,8-imide (ANI) in toluene as the standard ($\lambda_{\text{em}} = 495 \text{ nm}$; $\Phi_{\text{PL}} = 0.91$).⁴⁵ ^eSamples degassed using the freeze–pump–thaw technique. ^fExcited state emission lifetimes measured using time-correlated single-photon counting with pulsed laser diode excitation at 405 nm.

Considering that typical second- and third-row transition metal sensitizers exhibit only modest light absorption in the visible region,^{3,15,18,20,21} it is worth noting that S1–S3 are capable of light absorption across the majority of the visible spectrum (400–600 nm), with maxima at 514, 507, and 435 nm for S1–S3, respectively. The extinction coefficients at these respective maxima are on the order of $10^4 \text{ M}^{-1} \text{ cm}^{-1}$, which are similar to the intensities of the MLCT absorptions in transition metal complexes but can be readily tuned with facile structural modifications and can achieve significantly red-shifted absorption bands by comparison. Consequently, the total integrated intensity of the absorption spectra across the visible region is much larger for S1–S3, suggesting an advantage of using these chromophores over traditional metal-containing photosensitizers.

Chromophores P1–P3 exhibit intense fluorescence arising from the initially populated ${}^1(\pi \rightarrow \pi^*)$ excited state that decays within the early nanosecond time regime (Table 1). In addition to inducing significant bathochromic shifts to the electronic absorption spectra, S1–S3 also resulted in quantitative quenching of this prompt singlet fluorescence. Additionally, no photoluminescence was observed for any of the thionated perinone chromophores even at 77 K in 2-methyl-tetrahydrofuran, indicating the presence of substantial nonradiative deactivation channels. The observation of quantitatively quenched fluorescence was anticipated given the prediction of efficient triplet formation in these chromophores;^{27–29,31} however, the lack of phosphorescence even at 77 K encouraged us to measure singlet oxygen quantum yields to confirm triplet state formation as the dominant driver in excited state decay. The observation of singlet oxygen phosphorescence at $\sim 1270 \text{ nm}$ in aerated solutions of S1–S3 (Figure S21) confirmed the process of triplet formation.⁴⁶ To the best of our knowledge, this is the first report of accessing the triplet manifold in perinone chromophores without incorporating a third-row transition metal into the molecular architecture.⁴⁷ Furthermore, the singlet oxygen quantum yields [Φ_{Δ} (Table 2)] were measured

Table 2. Triplet-Based Photophysical Properties of Chromophores S1–S3^a

molecule	τ_{T} (298 K) ^{b,c} (μs)	Φ_{Δ} (298 K) ^d	E_{T} (eV) ^e
S1	0.664	0.78	1.53–1.77
S2	1.90	0.85	1.53–1.77
S3	12.9 ^f	1.0	1.77–2.00

^aMeasurements were performed in toluene. ^bExcited state TA lifetimes taken with an Edinburgh LP920 laser flash photolysis spectrometer. ^cSamples degassed using the freeze–pump–thaw technique. ^dSinglet oxygen quantum yields measured using aerated ZnTPP in toluene as the standard ($\Phi_{\Delta} = 0.93$).⁴⁶ ^eTriplet energies estimated using energy transfer quenching with a series of triplet acceptors (see the Supporting Information). ^fExcited state lifetime determined in the absence of self-quenching (theoretical infinite dilution) from concentration dependence (Figure S28).

as 0.78 for S1, 0.85 for S2, and 1.0 for S3, suggesting large triplet quantum yields (Φ_{T}) that rival those featured in transition metal complexes; the quantum yield of triplet state formation of S3 must be unity. The singlet oxygen phosphorescence signal was completely absent in aerated solutions of P1–P3, signifying that triplet state generation in S1–S3 was a direct consequence of a single thionation (Figures S22–S24). To glean more insight into the potential of S1–S3 as triplet photosensitizers, their triplet lifetimes were determined using nanosecond transient absorption spectroscopy, with the associated difference spectra presented in Figure 2A–C. The resultant single-exponential triplet lifetimes were measured as 0.664, 1.90, and 12.9 μs for S1, S2, and S3, respectively (Table 2).

In each case, the lifetimes of the thioperinones persisted into the microsecond time domain, which is sufficient to engage in bimolecular triplet sensitization. This process has yet to be demonstrated using perinone chromophores and is significantly underexplored using aromatic thiones in general. Therefore, we used S1–S3 to sensitize a series of pertinent PAH acceptors through TET under selective visible excitation (480 or 560 nm) of the thioperinone. Initially, a range of PAH acceptors were chosen for each thionated perinone to establish

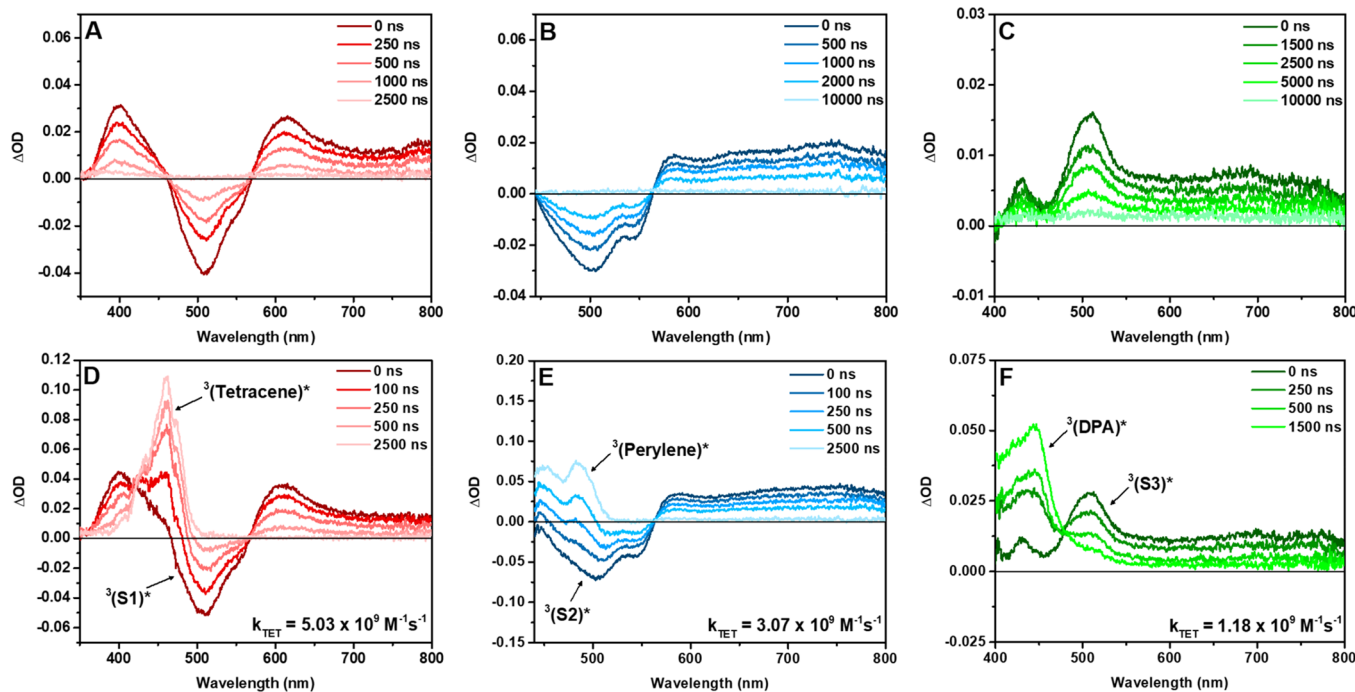


Figure 2. Nanosecond transient absorption difference spectra of (A) S1 (70 μ M), (B) S2 (90 μ M), and (C) S3 (50 μ M) without a quencher. Nanosecond transient absorption difference spectra of (D) S1 (70 μ M), (E) S2 (90 μ M), and (F) S3 (50 μ M) with tetracene (0.60 mM), perylene (0.40 mM), and DPA (1.30 mM) as quenchers, respectively. Transient spectra were recorded using 480 nm (S3) or 560 nm (S1 and S2) pulsed excitation (\sim 1.3–1.6 mJ/pulse, 7 ns full width at half-maximum) in deaerated toluene. The samples were deaerated using the freeze–pump–thaw method.

226 an estimate of their triplet energies because S1–S3 are not
 227 phosphorescent at 77 K, even when the glass-forming solvent
 228 was doped with an external heavy atom.⁴⁸ The resultant triplet
 229 energies are listed in Table 2 as 1.53–1.77 eV for S1 and S2
 230 and 1.77–2.0 eV for S3. A discussion of the experimental
 231 details and the triplet energy estimation procedure are reported
 232 in the Supporting Information.

233 The sensitized PAH triplets manifested in the TA difference
 234 spectra (Figure 2D–F) as characteristic peaks at 465 nm
 235 (tetracene), 480 nm (perylene), and 435 nm (DPA). The
 236 prompt signals in these transient spectra were dominated by
 237 contributions from each triplet $^3(\text{thioperinone})^*$, which then
 238 give rise to the $^3(\text{PAH})^*$ signal at longer delay times. The TET
 239 dynamics were monitored using Stern–Volmer quenching of
 240 the nanosecond TA kinetics (see the Supporting Information),
 241 with the resultant energy transfer rate constants (k_{TET})
 242 reported in Table 3. Comparison of TET dynamics across all
 243 three sensitizers indicated that the PAH acceptors with triplet
 244 energies of up to \sim 1.8 eV could be sensitized at the diffusion
 245 limit. Chromophore S3 was the only molecule that could
 246 effectively sensitize DPA (Figure 2F; $k_{\text{TET}} = 1.18 \times 10^9 \text{ M}^{-1} \text{ s}^{-1}$), while the lower triplet energies of S1 and S2 prevented a
 247 sufficient energetic driving force to facilitate the same process
 248 ($k_{\text{TET}} < 10^7 \text{ M}^{-1} \text{ s}^{-1}$). Thus, S1 and S2 served as ideal
 249 sensitizers for tetracene (Figure 2D; $k_{\text{TET}} = 5.03 \times 10^9 \text{ M}^{-1}$
 250 s^{-1}) and perylene (Figure 2E; $k_{\text{TET}} = 3.07 \times 10^9 \text{ M}^{-1} \text{ s}^{-1}$),
 251 respectively, due to the lower triplet energies of these PAHs.
 252 Because thionation was demonstrated to be an effective
 253 means for accessing the triplet manifold in perinones, we
 254 sought to elucidate the details of their electronic structures
 255 using DFT and TD-DFT calculations (M06-D3/Def-2-
 256 TZVP).^{49–53} The frontier molecular orbitals obtained from
 257 the ground state geometry optimizations of S1–S3 are shown

Table 3. TET Quenching of Chromophores S1–S3 as a Function of PAH Acceptor^a

sensitizer	acceptor	acceptor triplet energy (eV) ^b	$k_{\text{TET}} (\text{M}^{-1} \text{ s}^{-1})$
S1	tetracene	1.27	5.03×10^9
	perylene	1.53	1.89×10^8
	DPA	1.77	$<10^7$
S2	tetracene	1.27	4.74×10^9
	perylene	1.53	3.07×10^9
	DPA	1.77	$<10^7$
S3	perylene	1.53	7.48×10^9
	DPA	1.77	1.18×10^9
	pyrene	2.00	2.70×10^6

^aMeasurements were performed in deaerated toluene. Additional experimental details and kinetic data can be found in the Supporting Information. ^bAcceptor energies obtained from ref 1.

in Figure 3. For the low-lying singlet–singlet transitions, the HOMO, HOMO–1, and LUMO are the diagnostic orbitals for these chromophores. Throughout the series, the frontier orbitals feature HOMO and LUMO as π and π^* in character, respectively, and the HOMO–1 to be nonbonding in character, with most of the electron density centered on the sulfur atom. This is in stark contrast to P1–P3, which do not exhibit frontier molecular orbitals with any significant nonbonding character (Figure S38). Using TD-DFT, the transitions between the frontier orbitals of S1–S3 were calculated and are reported for the two lowest-lying singlet–singlet transitions (Table S2). For each chromophore, TD-DFT predicts the lowest energy singlet–singlet transition ($S_0 \rightarrow S_1$) to be an optically forbidden $n \rightarrow \pi^*$ transition, which was confirmed by the electron density difference surfaces generated from the optimized S1 structures (Figure S43). The

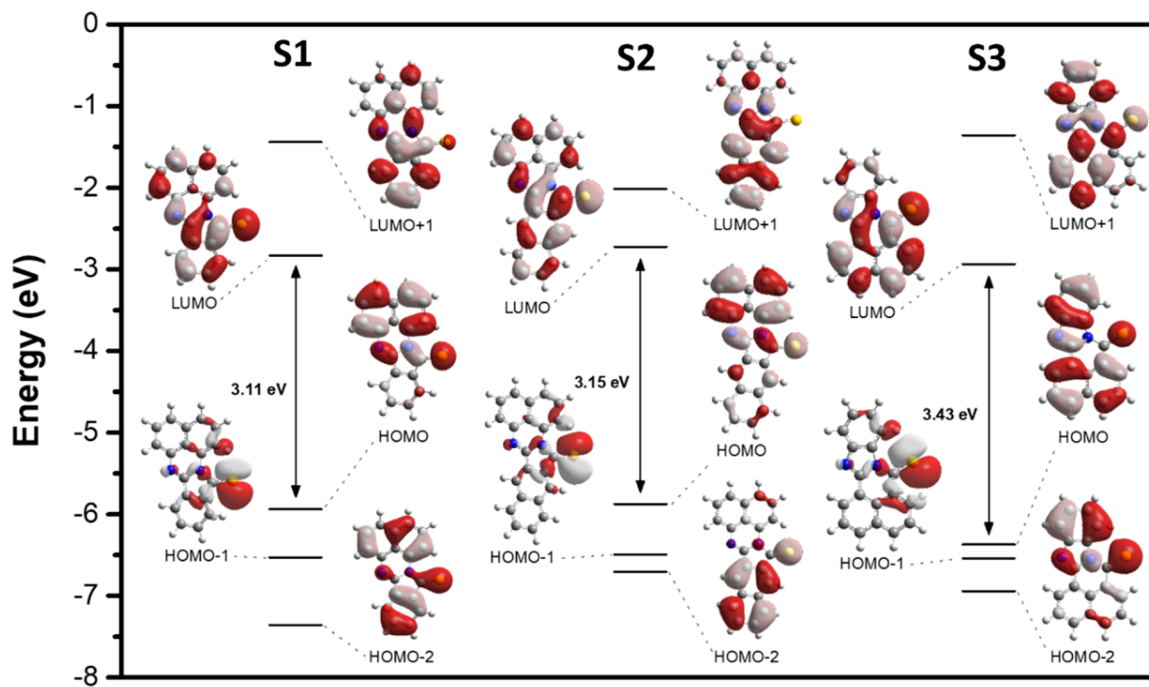


Figure 3. Frontier molecular orbital diagram of chromophores **S1–S3**. Calculations reveal the emergence of a nonbonding molecular orbital (HOMO-1) upon thionation when compared to the perinone models.

275 calculated $S_0 \rightarrow S_2$ transitions in chromophores **S1–S3** reveal
 276 these excitations to be intense $\pi \rightarrow \pi^*$ transitions, which
 277 correspond well with the experimentally observed $\lambda_{\text{abs max}}$ for
 278 the lowest energy absorbance bands (Figure S39). This result
 279 was expected given the similar appearance of the absorbance
 280 envelopes of chromophores **S1–S3** to their nonthionated
 281 parent chromophores **P1–P3**.

282 The assignment of S_1 as $n \rightarrow \pi^*$ and S_2 as $\pi \rightarrow \pi^*$ is widely
 283 established for numerous aromatic thioketones.^{27,42,43,54–58}
 284 However, whereas the $S_1 - S_2$ energy gap is large in most of
 285 these cases, the energetic proximity of the S_1 and S_2 excited
 286 states in **S1–S3** was revealed through electronic structure
 287 calculations (Table S2). Consequently, we anticipated that the
 288 much larger singlet–triplet splitting energy (ΔE_{ST}) of the $\pi \rightarrow$
 289 π^* configuration may cause inversion of the corresponding $^3(n$
 290 $\rightarrow \pi^*)$ and $^3(\pi \rightarrow \pi^*)$ excited states, similar to what has been
 291 proposed for thionated PDIs²⁷ and squarine dyes.³² Thus, we
 292 were motivated to perform natural transition orbital (NTO)
 293 analysis on the low-lying triplet manifold of chromophores
 294 **S1–S3** (Figures S40–S42). The $S_0 \rightarrow T_1$ NTOs display that
 295 the hole and electron reside mainly in the π system in
 296 chromophores **S1–S3** (i.e., T_1 can be described as $\pi \rightarrow \pi^*$ in
 297 all cases). The $S_0 \rightarrow T_2$ NTOs show that the hole resides in the
 298 nonbonding orbital centered on the sulfur atom, while the
 299 electron resides mainly in the π system in chromophores **S1–**
 300 **S3** (i.e., T_2 can be described as $n \rightarrow \pi^*$ in all cases). These
 301 results are supported by the triplet spin densities from the
 302 optimized T_1 states (Figure S43), confirming the suspected
 303 energetic inversion of the two lowest energy triplet excited
 304 states with respect to their corresponding singlet excited states.
 305 As a result of triplet state inversion, the difference in ISC
 306 efficiencies between the thionated and nonthionated perinones
 307 can be rationalized according to the El Sayed selection rules.⁵⁹
 308 These ISC selection rules state that an $S_1(n-\pi^*) \rightarrow T_1(\pi-\pi^*)$
 309 transition is allowed because the change in multiplicity is
 310 coupled with a change in symmetry, thus conserving the total

311 angular momentum of the interacting excited states. Similar 311
 312 observations of this $S_1(n-\pi^*) \rightarrow T_1(\pi-\pi^*)$ transition have 312
 313 also been established for the thionated squarine dyes discussed 313
 314 previously.³² Note that ISC to upper $^3(\pi \rightarrow \pi^*)$ excited states 314
 315 (T₃ and above) has been ruled out because they are 315
 316 significantly higher in energy with respect to S_1 , preventing 316
 317 an adequate driving force to enable efficient triplet state 317
 318 formation. While the nature and alignment of the singlet and 318
 319 triplet manifolds facilitate enhanced SOC in **S1–S3** via the El 319
 320 Sayed rules, the presence of solely $\pi \rightarrow \pi^*$ transitions in the 320
 321 low-lying singlet manifolds (Figure S38 and Table S3) of 321
 322 chromophores **P1–P3** illustrates why the model perinones 322
 323 exhibit comparatively inefficient ISC dynamics. Thus, the two 323
 324 main design criteria that allow efficient triplet formation in 324
 325 **S1–S3** can be generalized from these results: (1) these systems 325
 326 contain two lowest-lying singlet excited states in energetic 326
 327 proximity, where the higher energy configuration allows a 327
 328 larger exchange interaction due to the superior overlap density 328
 329 of participating orbitals, and (2) these singlet states possess 329
 330 different symmetries, facilitating SOC via the El Sayed rules. A 330
 331 representative summary of these criteria as they apply to **S3** is 331
 332 shown in Figure 4, along with the associated photophysical 332 f4
 333 properties.

334 As mentioned previously, sensitization of various PAH 334
 335 acceptors has pivotal implications in TTA-UC and photoredox 335
 336 catalysis, where costly second- and third-row transition metal 336
 337 complexes currently dominate as triplet sensitizers. Sensitiza- 337
 338 tion of DPA and other anthracene derivatives by **S3** is 338
 339 particularly attractive for sensitization-initiated electron trans- 339
 340 fer (SenI-ET) in photoredox catalysis.⁷ Sensitized $^3(\text{DPA})^*$ 340
 341 can be reduced by sacrificial electron donors to generate highly 341
 342 reductive radical anions (-1.94 vs SCE),¹ which are capable of 342
 343 activating various stable substrates for the construction of 343
 344 challenging carbon–carbon and carbon–heteroatom bonds.⁷ 344
 345 Thus, replacement of archetypal photoredox catalysts such as 345
 346 $\text{Ru}(\text{bpy})_3^{2+}$ or *fac*-Ir(*ppy*)₃ with **S3**/DPA can substantially 346

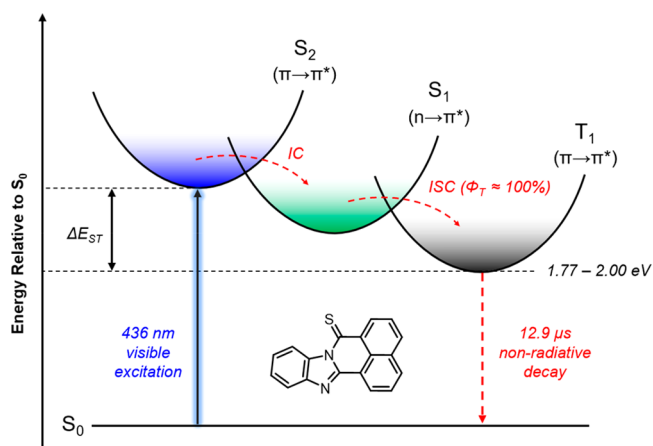


Figure 4. Proposed mechanism for excited state decay through the triplet manifold for chromophore S3 and associated photophysical data. Only the most probable electronic transitions are shown.

alleviate scalability barriers in the catalytic activation of many organic molecules.⁶⁰ SenI-ET using S3/DPA is also an attractive replacement for many totally organic photoredox catalysts, which often absorb strongly only in the ultraviolet.⁶¹ As an alternative to photoredox catalysis, chromophores S1 and S2 can readily serve as candidates for green-to-blue upconversion schemes using perylene as an acceptor/annihilator.⁶² In these cases, excitation over a range of green wavelengths (500–580 nm) can potentially facilitate upconverted blue fluorescence and an anti-Stokes shift of up to ~0.6 eV, which is typically achieved using expensive Pt(II)-porphyrin or polypyridyl complexes as photosensitizers.^{4,6} Upconversion schemes such as this may have further implications in energy conversion processes allowing sub-band gap harnessing of solar photons in photovoltaics, a crucial step toward breaching the Shockley–Queisser efficiency limit.⁶³ Clearly, PAHs are used pervasively throughout the literature as molecular acceptors, which is why these molecules were chosen to emphasize the applicability of S1–S3 as photosensitizers. However, other acceptors, such as common BODIPY dyes used in TTA-UC schemes,⁶ represent viable candidates to pair with S1–S3 as sensitizers. Furthermore, the notably high singlet oxygen quantum yields of S1–S3 make them promising sensitizers for photodynamic therapy, particularly when visible-light excitation is required.²⁸

In summary, we have demonstrated the first comprehensive design and implementation of metal-free triplet photosensitizers using the perinone molecular framework. Highly desirable red-shifted absorbance bands that maintain intense molar extinction coefficients across the visible region were achieved through a one-step thionation, which were also accompanied by efficient population of the triplet manifold inferred from the quantum yields for singlet oxygen formation ($\Phi_{\Delta} = 0.78–1.0$). Consequently, the excited state lifetimes of the perinone chromophores were extended into the microsecond time domain, allowing effective bimolecular triplet sensitization of PAH acceptors with triplet energies of up to ~1.8 eV. Finally, we characterized the nature of the electronic structure that facilitates efficient triplet formation in thionated perinones and generalized an emerging design approach for metal-free triplet photosensitizers. As emphasized above, using totally organic triplet photosensitizers can substantially reduce the cost of many bimolecular photochemical and photo-

physical transformations that currently utilize transition metal photosensitizers. This is particularly evident when considering species such as platinum porphyrins and benchmark ruthenium(II) polypyridine complexes, which have been commonly used as sensitizers for solar-based TTA-UC^{2,4,19} or photochemical reactions.^{3,7} Because of the transition from small laboratory investigations to industrial processes required to serve the general public, scalability costs become a primary issue. Additionally, most transition metal-based sensitizers rely on selective excitation into MLCT states with fairly weak absorption in the visible region,^{3,15,18,20,21} which implies that excess material is required for maximum photon absorption at visible wavelengths. Thus, we believe that the tailored design of thionated perinone chromophores enables them to serve as potential replacements for precious transition metal photosensitizers in applications where energy is extracted from the triplet state under visible-light excitation.

ASSOCIATED CONTENT

Supporting Information

The Supporting Information is available free of charge at <https://pubs.acs.org/doi/10.1021/acs.jpcllett.0c01634>.

Experimental methods, structural characterization data, additional static and time-resolved spectra, additional electronic structure calculation details, and the three-dimensional structures (XYZ) of S1–S3 (PDF)

AUTHOR INFORMATION

Corresponding Author

Felix N. Castellano — Department of Chemistry, North Carolina State University, Raleigh, North Carolina 27695-8204, United States;  orcid.org/0000-0001-7546-8618; Phone: (919) 515-3021; Email: fncastel@ncsu.edu

Authors

Jonathan R. Palmer — Department of Chemistry, North Carolina State University, Raleigh, North Carolina 27695-8204, United States

Kaylee A. Wells — Department of Chemistry, North Carolina State University, Raleigh, North Carolina 27695-8204, United States;  orcid.org/0000-0002-6870-6574

James E. Yarnell — Department of Chemistry, North Carolina State University, Raleigh, North Carolina 27695-8204, United States; Department of Chemistry & Chemistry Research Center, United States Air Force Academy, Colorado Springs, Colorado 80840-6230, United States;  orcid.org/0000-0003-0049-9887

Joseph M. Favale — Department of Chemistry, North Carolina State University, Raleigh, North Carolina 27695-8204, United States

Complete contact information is available at: <https://pubs.acs.org/10.1021/acs.jpcllett.0c01634>

Notes

The authors declare no competing financial interest.

ACKNOWLEDGMENTS

This work was supported by the U.S. Department of Energy, Office of Science, Office of Basic Energy Sciences, under Award DE-SC0011979. J.E.Y. was supported by the Air Force Institute of Technology (AFIT), and K.A.W. was supported by the National Science Foundation (CHE-1665033).

447 ■ REFERENCES

448 (1) Montalti, M.; Credi, A.; Prodi, L.; Gandolfi, M. T. *Handbook of*
449 *photochemistry*, 3rd ed.; CRC/Taylor & Francis: Boca Raton, FL,
450 2006.

451 (2) Cheng, Y. Y.; Fückel, B.; MacQueen, R. W.; Khoury, T.; Clady,
452 R. G. C. R.; Schulze, T. F.; Ekins-Daukes, N. J.; Crossley, M. J.;
453 Stannowski, B.; Lips, K.; Schmidt, T. W. Improving the light-
454 harvesting of amorphous silicon solar cells with photochemical
455 upconversion. *Energy Environ. Sci.* **2012**, *5*, 6953–6959.

456 (3) Islangulov, R. R.; Castellano, F. N. Photochemical upconversion:
457 anthracene dimerization sensitized to visible light by a Ru^{II}
458 chromophore. *Angew. Chem., Int. Ed.* **2006**, *45*, 5957–5959.

459 (4) Schulze, T. F.; Schmidt, T. W. Photochemical upconversion:
460 present status and prospects for its application to solar energy
461 conversion. *Energy Environ. Sci.* **2015**, *8*, 103–125.

462 (5) Cheng, Y. Y.; Khoury, T.; Clady, R. G. C. R.; Tayebjee, M. J. Y.;
463 Ekins-Daukes, N. J.; Crossley, M. J.; Schmidt, T. W. On the efficiency
464 limit of triplet-triplet annihilation for photochemical upconversion.
465 *Phys. Chem. Chem. Phys.* **2010**, *12*, 66–71.

466 (6) Singh-Rachford, T. N.; Castellano, F. N. Photon upconversion
467 based on sensitized triplet-triplet annihilation. *Coord. Chem. Rev.*
468 **2010**, *254*, 2560–2573.

469 (7) Ghosh, I.; Shaikh, R. S.; König, B. Sensitization-initiated electron
470 transfer for photoredox catalysis. *Angew. Chem., Int. Ed.* **2017**, *56*,
471 8544–8549.

472 (8) Ravetz, B. D.; Pun, A. B.; Churchill, E. M.; Congreve, D. N.;
473 Rovis, T.; Campos, L. M. Photoredox catalysis using infrared light via
474 triplet fusion upconversion. *Nature* **2019**, *S65*, 343–346.

475 (9) Pal, A. K.; Li, C.; Hanan, G. S.; Zysman-Colman, E. Blue-
476 emissive cobalt(III) complexes and their use in the photocatalytic
477 trifluoromethylation of polycyclic aromatic hydrocarbons. *Angew.*
478 *Chem., Int. Ed.* **2018**, *57*, 8027–8031.

479 (10) Yost, S. R.; Lee, J.; Wilson, M. W. B.; Wu, T.; McMahon, D. P.;
480 Parkhurst, R. R.; Thompson, N. J.; Congreve, D. N.; Rao, A.; Johnson,
481 K.; Sfeir, M. Y.; Bawendi, M. G.; Swager, T. M.; Friend, R. H.; Baldo,
482 M. A.; Van Voorhis, T. A transferable model for singlet-fission
483 kinetics. *Nat. Chem.* **2014**, *6*, 492–497.

484 (11) Wilson, M. W. B.; Rao, A.; Johnson, K.; Gélinas, S.; di Pietro,
485 R.; Clark, J.; Friend, R. H. Temperature-independent singlet exciton
486 fission in tetracene. *J. Am. Chem. Soc.* **2013**, *135*, 16680–16688.

487 (12) Willems, R. E. M.; Meskers, S. C. J.; Wienk, M. M.; Janssen, R.
488 A. J. Effect of charge-transfer state energy on charge generation
489 efficiency via singlet fission in pentacene-fullerene solar cells. *J. Phys.*
490 *Chem. C* **2019**, *123*, 10253–10261.

491 (13) Sanders, S. N.; Kumarasamy, E.; Pun, A. B.; Trinh, M. T.; Choi,
492 B.; Xia, J.; Taffet, E. J.; Low, J. Z.; Miller, J. R.; Roy, X.; Zhu, X. Y.;
493 Steigerwald, M. L.; Sfeir, M. Y.; Campos, L. M. Quantitative
494 intramolecular singlet fission in bipentacenes. *J. Am. Chem. Soc.*
495 **2015**, *137*, 8965–8972.

496 (14) Sanders, S. N.; Kumarasamy, E.; Pun, A. B.; Appavoo, K.;
497 Steigerwald, M. L.; Campos, L. M.; Sfeir, M. Y. Exciton correlations in
498 intramolecular singlet fission. *J. Am. Chem. Soc.* **2016**, *138*, 7289–
499 7297.

500 (15) Guo, X.; Liu, Y.; Chen, Q.; Zhao, D.; Ma, Y. New
501 bichromophoric triplet photosensitizer designs and their application
502 in triplet-triplet annihilation upconversion. *Adv. Opt. Mater.* **2018**, *6*,
503 1700981.

504 (16) Zhao, J.; Wu, W.; Sun, J.; Guo, S. Triplet photosensitizers: from
505 molecular design to applications. *Chem. Soc. Rev.* **2013**, *42*, 5323–
506 5351.

507 (17) Zhao, J.; Chen, K.; Hou, Y.; Che, Y.; Liu, L.; Jia, D. Recent
508 progress in heavy atom-free organic compounds showing unexpected
509 intersystem crossing (ISC) ability. *Org. Biomol. Chem.* **2018**, *16*,
510 3692–3701.

511 (18) Zhao, J.; Ji, S.; Wu, W.; Wu, W.; Guo, H.; Sun, J.; Sun, H.; Liu,
512 Y.; Li, Q.; Huang, L. Transition metal complexes with strong
513 absorption of visible light and long-lived triplet excited states: from
514 molecular design to applications. *RSC Adv.* **2012**, *2*, 1712–1728.

515 (19) Islangulov, R. R.; Kozlov, D. V.; Castellano, F. N. Low power
516 upconversion using MLCT sensitizers. *Chem. Commun.* **2005**, *3776–*
517 3778.

518 (20) Zhao, W.; Castellano, F. N. Upconverted emission from pyrene
519 and di-tert-butylpyrene using Ir(ppy)₃ as triplet sensitizer. *J. Phys. Chem. A* **2006**, *110*, 11440–11445.

520 (21) Du, P.; Eisenberg, R. Energy upconversion sensitized by a
521 platinum(II) terpyridyl acetylide complex. *Chem. Sci.* **2010**, *1*, 502–
522 506.

523 (22) Yarnell, J. E.; Deaton, J. C.; McCusker, C. E.; Castellano, F. N.
524 Bidirectional “ping-pong” energy transfer and 3000-fold lifetime
525 enhancement in a Re(I) charge transfer complex. *Inorg. Chem.* **2011**, *50*,
526 7820–7830.

527 (23) Yarnell, J. E.; Wells, K. A.; Palmer, J. R.; Breaux, J. M.;
528 Castellano, F. N. Excited-state triplet equilibria in a series of Re(I)-
529 naphthalimide bichromophores. *J. Phys. Chem. B* **2019**, *123*, 7611–
530 7627.

531 (24) Tyson, D. S.; Bialecki, J.; Castellano, F. N. Ruthenium(II)
532 complex with a notably long excited state lifetime. *Chem. Commun.*
533 **2000**, 2355–2356.

534 (25) Tyson, D. S.; Castellano, F. N. Light-harvesting arrays with
535 coumarin donors and MLCT acceptors. *Inorg. Chem.* **1999**, *38*, 4382–
536 4383.

537 (26) Tyson, D. S.; Luman, C. R.; Zhou, X.; Castellano, F. N. New
538 Ru(II) chromophores with extended excited-state lifetimes. *Inorg.*
539 *Chem.* **2001**, *40*, 4063–4071.

540 (27) Tilley, A. J.; Pensack, R. D.; Lee, T. S.; Djukic, B.; Scholes, G.
541 D.; Seferos, D. S. Ultrafast triplet formation in thionated perylene
542 diimides. *J. Phys. Chem. C* **2014**, *118*, 9996–10004.

543 (28) Nguyen, V.-N.; Qi, S.; Kim, S.; Kwon, N.; Kim, G.; Yim, Y.;
544 Park, S.; Yoon, J. An emerging molecular design approach to heavy-
545 atom-free photosensitizers for enhanced photodynamic therapy under
546 hypoxia. *J. Am. Chem. Soc.* **2019**, *141*, 16243–16248.

547 (29) Nguyen, V.-N.; Baek, G.; Qi, S.; Heo, S.; Yim, Y.; Yoon, J. A
548 lysosome-localized thionaphthalimide as a potential heavy-atom-free
549 photosensitizer for selective photodynamic therapy. *Dyes Pigm.* **2020**, *550*
551 177, 108265.

552 (30) Zhang, L.; Huang, Z.; Dai, D.; Xiao, Y.; Lei, K.; Tan, S.; Cheng,
553 J.; Xu, Y.; Liu, J.; Qian, X. Thio-bisnaphthalimides as heavy-atom-free
554 photosensitizers with efficient singlet oxygen generation and large
555 Stokes shifts: synthesis and properties. *Org. Lett.* **2016**, *18*, 5664–
556 5667.

557 (31) Peceli, D.; Hu, H.; Fishman, D. A.; Webster, S.; Przhonska, O.
558 V.; Kurdyukov, V. V.; Slominsky, Y. L.; Tolmachev, A. I.; Kachkovski,
559 A. D.; Gerasov, A. O.; Masunov, A. E.; Hagan, D. J.; Van Stryland, E.
560 W. Enhanced intersystem crossing rate in polymethine-like molecules:
561 sulfur-containing squaraines versus oxygen-containing analogues. *J. Phys.*
562 *Chem. A* **2013**, *117*, 2333–2346.

563 (32) Webster, S.; Peceli, D.; Hu, H.; Padilha, L. A.; Przhonska, O.
564 V.; Masunov, A. E.; Gerasov, A. O.; Kachkovski, A. D.; Slominsky, Y.
565 L.; Tolmachev, A. I.; Kurdyukov, V. V.; Viniychuk, O. O.; Barrasso,
566 E.; Lepkowicz, R.; Hagan, D. J.; Van Stryland, E. W. Near-unity
567 quantum yields for intersystem crossing and singlet oxygen generation
568 in polymethine-like molecules: design and experimental realization. *J.*
569 *Phys. Chem. Lett.* **2010**, *1*, 2354–2360.

570 (33) Pristash, S. R.; Corp, K. L.; Rabe, E. J.; Schlenker, C. W. Heavy-
571 atom-free red-to-yellow photon upconversion in a thiosquaraine
572 composite. *ACS Appl. Energy Mater.* **2020**, *3*, 19–28.

573 (34) Debjie, M. G.; Verbunt, P. P. C.; Nadkarni, P. J.; Velate, S.;
574 Bhaumik, K.; Nedumbamana, S.; Rowan, B. C.; Richards, B. S.;
575 Hoeks, T. L. Promising fluorescent dye for solar energy conversion
576 based on a perylene perinone. *Appl. Opt.* **2011**, *50*, 163–169.

577 (35) Kobraček, K. I.; Zubková, N. S.; Stankevič, G. S.; Šestakova,
578 Y. S.; Stroganov, V. S.; Adrov, O. I. New aryleneimidazoles as dyes
579 for thermoplastic polymeric materials. *Fibre Chem.* **2006**, *38*, 183–
580 187.

581 (36) Mamada, M.; Pérez-Bolívar, C.; Kumaki, D.; Esipenko, N. A.;
582 Tokito, S.; Anzenbacher, P., Jr. Benzimidazole derivatives: synthesis,
583

583 physical properties, and n-type semiconducting properties. *Chem. -*
584 *Eur. J.* **2014**, *20*, 11835–11846.

585 (37) Loufty, R. O.; Hor, A. M.; Kazmaier, P. M.; Burt, R. A.; Hamer,
586 G. K. Organic photoconductive (OPC) devices incorporating
587 bisarylimidazole perinone pigments. *Dyes Pigm.* **1991**, *15*, 139–156.

588 (38) Mamada, M.; Pérez-Bolívar, C.; Anzenbacher, P. Green
589 synthesis of polycyclic benzimidazole derivatives and organic
590 semiconductors. *Org. Lett.* **2011**, *13*, 4882–4885.

591 (39) Law, K. Y. Organic photoconductive materials: recent trends
592 and developments. *Chem. Rev.* **1993**, *93*, 449–486.

593 (40) Nagao, Y. Synthesis and properties of perylene pigments. *Prog.*
594 *Org. Coat.* **1997**, *31*, 43–49.

595 (41) Pahlavanlu, P.; Tilley, A. J.; McAllister, B. T.; Seferos, D. S.
596 Microwave synthesis of thionated naphthalene diimide-based small
597 molecules and polymers. *J. Org. Chem.* **2017**, *82*, 12337–12345.

598 (42) Coyle, J. D. The photochemistry of thiocarbonyl compounds.
599 *Tetrahedron* **1985**, *41*, 5393–5425.

600 (43) Maciejewski, A.; Steer, R. P. The photophysics, physical
601 photochemistry, and related spectroscopy of thiocarbonyls. *Chem. Rev.*
602 **1993**, *93*, 67–98.

603 (44) Suzuki, K.; Kobayashi, A.; Kaneko, S.; Takehira, K.; Yoshihara,
604 T.; Ishida, H.; Shiina, Y.; Oishi, S.; Tobita, S. Reevaluation of absolute
605 luminescence quantum yields of standard solutions using a
606 spectrometer with an integrating sphere and a back-thinned CCD
607 detector. *Phys. Chem. Chem. Phys.* **2009**, *11*, 9850–9860.

608 (45) Greenfield, S. R.; Svec, W. A.; Gosztola, D.; Wasielewski, M. R.
609 Multistep photochemical charge separation in rod-like molecules
610 based on aromatic imides and diimides. *J. Am. Chem. Soc.* **1996**, *118*,
611 6767–6777.

612 (46) Wilkinson, F.; Helman, W. P.; Ross, A. B. Quantum yields for
613 the photosensitized formation of the lowest electronically excited
614 singlet state of molecular oxygen in solution. *J. Phys. Chem. Ref. Data*
615 **1993**, *22*, 113–262.

616 (47) Yarnell, J. E.; De La Torre, P.; Castellano, F. N. Efficient
617 phosphorescence from naphthalenebenzimidizole-coordinated
618 iridium(III) chromophores. *Eur. J. Inorg. Chem.* **2017**, *2017*, 5238–
619 5245.

620 (48) Kondakova, M. E.; Pawlik, T. D.; Young, R. H.; Giesen, D. J.;
621 Kondakov, D. Y.; Brown, C. T.; Deaton, J. C.; Lenhard, J. R.; Klubek,
622 K. P. High-efficiency, low-voltage phosphorescent organic light-
623 emitting diode devices with mixed host. *J. Appl. Phys.* **2008**, *104*,
624 094501.

625 (49) Zhao, Y.; Truhlar, D. G. The M06 suite of density functionals
626 for main group thermochemistry, thermochemical kinetics, non-
627 covalent interactions, excited states, and transition elements: two new
628 functionals and systematic testing of four M06-class functionals and
629 12 other functionals. *Theor. Chem. Acc.* **2008**, *120*, 215–241.

630 (50) Weigend, F.; Ahlrichs, R. Balanced basis sets of split valence,
631 triple zeta valence and quadruple zeta valence quality for H to Rn:
632 design and assessment of accuracy. *Phys. Chem. Chem. Phys.* **2005**, *7*,
633 3297–3305.

634 (51) Weigend, F. Accurate Coulomb-fitting basis sets for H to Rn.
635 *Phys. Chem. Chem. Phys.* **2006**, *8*, 1057–1065.

636 (52) Cossi, M.; Scalmani, G.; Rega, N.; Barone, V. New
637 developments in the polarizable continuum model for quantum
638 mechanical and classical calculations on molecules in solution. *J.*
639 *Chem. Phys.* **2002**, *117*, 43–54.

640 (53) Krieg, H.; Antony, J.; Ehrlich, S.; Grimme, S. A consistent and
641 accurate ab initio parametrization of density functional dispersion
642 correction (DFT-D) for the 94 elements H–Pu. *J. Chem. Phys.* **2010**,
643 *132*, 154104.

644 (54) Steer, R. P. Structure and decay dynamics of electronic excited
645 states of thiocarbonyl compounds. *Rev. Chem. Intermed.* **1981**, *4*, 1–
646 41.

647 (55) Szymanski, M.; Maciejewski, A.; Steer, R. P. Concerning
648 apparent intersystem crossing efficiencies in molecules with small S_1 -
649 T_1 energy gaps. *J. Photochem. Photobiol. A* **1991**, *57*, 405–418.

(56) Maciejewski, A.; Szymanski, M.; Steer, R. P. Thermally activated delayed S1 fluorescence of aromatic thiones. *J. Phys. Chem.* **1986**, *90*, 6314–6318.

(57) Maciejewski, A.; Szymanski, M.; Steer, R. P. T_1 – T_2 inversion in aromatic thiones. *Chem. Phys. Lett.* **1988**, *143*, 559–564.

(58) Szymański, M.; Maciejewski, A.; Steer, R. P. Photophysics of thione triplets in solution: factors controlling the rates of radiationless decay. *Chem. Phys.* **1988**, *124*, 143–154.

(59) El-Sayed, M. A. Spin-orbit coupling and the radiationless processes in nitrogen heterocyclics. *J. Chem. Phys.* **1963**, *38*, 2834–2838.

(60) Prier, C. K.; Rankic, D. A.; MacMillan, D. W. C. Visible light photoredox catalysis with transition metal complexes: applications in organic synthesis. *Chem. Rev.* **2013**, *113*, 5322–5363.

(61) Romero, N. A.; Nicewicz, D. A. Organic photoredox catalysis. *Chem. Rev.* **2016**, *116*, 10075–10166.

(62) Wu, W.; Guo, H.; Wu, W.; Ji, S.; Zhao, J. Organic triplet sensitizer library derived from a single chromophore (BODIPY) with long-lived triplet excited state for triplet-triplet annihilation based upconversion. *J. Org. Chem.* **2011**, *76*, 7056–7064.

(63) Tayebjee, M. J. Y.; McCamey, D. R.; Schmidt, T. W. Beyond Shockley-Queisser: molecular approaches to high-efficiency photo voltaics. *J. Phys. Chem. Lett.* **2015**, *6*, 2367–2378.